Flux estimates of ions from the lunar exosphere

M. Sarantos[1,2,3], R.E. Hartle [1,3], R.M. Killen [4,3], Y. Saito[5], J.A. Slavin[6], and A. Glocer[1]

(1) Heliophysics Science Division, NASA Goddard Space Flight Center, Greenbelt, MD, USA

(2) Goddard Planetary Heliophysics Institute, University of Maryland, Baltimore County, Baltimore, MD, USA

(3) NASA Lunar Science Institute, NASA Ames Research Center, Moffett Field, CA, USA

(4) Planetary Magnetospheres Branch, NASA Goddard Space Flight Center, Greenbelt, MD, USA

(5) Institute of Space and Astronautical Science, Japan Aerospace Exploration Agency, 3-1-1 Yoshinodai, Chuo-ku, Sagamihara, Kanagawa 252-5210, Japan

(6) Department of Atmospheric, Oceanic and Space Sciences, University of Michigan, Ann Arbor, MI, USA

Abstract

We compare estimates for the ion fluxes of twelve expected constituents of the lunar exosphere with estimates for the ion fluxes ejected from the lunar surface by solar wind ions and electrons. Our estimates demonstrate that measurements of lunar ions will help constrain the abundances of many undetected species in the lunar exosphere, particularly Al and Si, because the expected ion flux levels from the exosphere exceed those from the surface. To correctly infer the relative abundances of exospheric ions and neutrals from Kaguya Ion Mass Analyzer (IMA) measurements, we must take into account the velocity distributions of local ions. The predicted spectrum underestimates the measured levels of O^+ relative to other lunar ion species, a result that may suggest contributions by molecular ions to the measured O^+ rates.

34 1. Introduction

35

36 The Earth's Moon is surrounded by a thin exosphere many of whose expected
37 neutral constituents remain undetected [*Stern*, 1999]. The unknown constituents of the
38 lunar exosphere can be probed by measurements of pickup ions, which are often easier to
39 detect owing to the high sensitivity of ion mass spectrometers. Many ion species have
40 been detected at the Moon although their neutrals have not. Lunar ions have been
41 observed by the AMPTE [*Hilchenbach et al, 1991*], WIND [*Mall et al., 1998*], and
42 SELENE (Kaguya) [*Yokota et al., 2009; Tanaka et al., 2009*] spacecraft. Such ions can
43 be created not only by photoionization of exospheric neutrals, but also directly sputtered
44 from the lunar surface during its bombardment by solar wind ions and electrons [*Elphic*
45 *et al, 1991; McLain et al., 2011*].

46 The relative importance of these two sources of ions, the surface and the neutral
47 exosphere, is unclear. In principle, ions from the surface and ions from the exosphere can
48 be distinguished by their distinctive energy spectra: the surface ions are nearly
49 monoenergetic, while some exo-ion species may have a more extended energy range
50 [*Yokota and Saito, 2005*], depending on the ratio of ion gyroradius to neutral scale height
51 [*Hartle and Killen*, 2006].However, it is difficult to quantify the different ion sources
52 directly from measurements because surface ions can only be detected by spacecraft on
53 the side of the Moon that lies in the direction of the solar wind electric field, whereas ions
54 from the exosphere are more widely distributed [*Hartle and Killen, 2006*]. Therefore,
55 self-consistent models for the expected neutral and exo-ion abundances are required to

clarify the likelihood of inferring neutral abundances for each species from ion measurements.

Abundances of twelve ion species of exospheric origin (He^+, C^+, O^+, Na^+, Mg^+, Si^+, Al^+, S^+, Ca^+, K^+, Ti^+ and Fe^+) are estimated herein, most of them for the first time. Our predictions are based on models for lunar exospheric neutrals [*Hartle and Thomas, 1974; Sarantos et al., 2010; Sarantos et al., 2012*] that were validated with existing observations (detections for He, Na and K; upper limits for other species). With these production rates, dependent on altitude and zenith angle, we initialized an ion transport model [*Hartle et al., 2011*] to quantify fluxes of lunar pickup ions from exospheric sources. These rates were compared to the expected rates of secondary ions emitted from the surface by sputtering and electron stimulated desorption. Last, because ions near the Moon may be highly directional, we studied how exo-ions map into a detector that does not have a 4π field-of-view. This last part is specifically relevant to interpreting published measurements by Kaguya, because its time-of-flight Ion Mass Analyzer (IMA) is turned towards the Moon with a 2π field-of-view [*Yokota et al., 2009; Tanaka et al., 2009; Saito et al., 2010*].

2. Observations

Lunar ions have been observed far downstream of the Moon and, more recently, near the Moon. The first ions of lunar origin were detected by the time-of-flight spectrometer onboard the AMPTE spacecraft; they were dominated by peaks corresponding to Si^+ and/or Al^+, with a secondary peak at O^+ [*Hilchenbach et al.*, 1991]. Lunar ions were also detected during lunar swingbys of the WIND spacecraft well

upstream from Earth, yielding once again clear peaks due to O^+, Si^+ and Al^+, with oxygen being most prominent [*Mall et al., 1998*]. The observed O^+ could be attributed neither to magnetospheric nor to interstellar origin. More recently, pickup ions were observed at altitudes ~100 km above the Moon from the MAP-PACE-IMA spectrometer onboard the SELENE (Kaguya) lunar orbiter. When the Moon was in the solar wind, *Yokota et al.* [2009] reported the detection of He^+, C^+, O^+, Na^+, and K^+. In addition, when the Moon was in the magnetosphere, *Tanaka et al.* [2009] reported the presence of H^+, He^{++}, He^+, C^+, O^+, Na^+, K^+ and Ar^+. Such ions could be a mix of solar wind, outflow from Earth's ionosphere, and of lunar origin.

Ions desorbed from the lunar surface can be constrained by laboratory experiments. When lunar soil simulants were bombarded by solar wind-like ions in Secondary Ion Mass Spectrometry (SIMS) experiments, significant fluxes of secondary lunar ions were ejected (~10^3–10^4 ions cm^{-2} s^{-1} if the typical solar wind flux of 4×10^8 ions cm^{-2} s^{-1} is assumed) [*Elphic et al.*, 1991]. Yields were higher for elements with lower ionization potentials such as K^+, Na^+, Ca^+, and Al^+. Experiments of electron impact onto Na and K bearing glasses indicated that Electron-Stimulated Desorption (ESD) produces ions [*McLain et al.*, 2011]. Measured ESD yields for 1 keV electrons were ~ 10^{-3} ions/electron, so the typical fluxes of electrons in the solar wind could result in a flux of ~10^5 total ions (summed over all species) per cm^{-2} s^{-1} from the lunar surface. Hence, the expected fluxes of surface ions from ESD and sputtering may be comparable in magnitude. ESD yields were found by *McLain et al.* [2011] to depend on substrate temperature, and hence on solar zenith angle. Owing to their dependence on the solar

wind incidence angle, sputtered ions will also have a solar zenith angle dependence, as will ions originating from the exosphere.

3. Integrated model of lunar neutrals and ions

The lunar atmosphere can be produced by a variety of source processes: thermal and photon-stimulated desorption (PSD), micrometeroid impact vaporization, and solar wind sputtering [*Stern*, 1999]. The resulting gas populations exhibit a mix of thermal (or *accommodated* to the lunar surface temperature) and non-thermal velocity distributions. The altitude dependence of exospheric neutrals, a reflection of the ejection processes, is expected theoretically to control the distributions of resulting ions above the Moon [*Hartle and Killen* 2006; *Hartle et al.*, 2011].

The exospheric abundances of neutral He, Na, and K are known from measurements. We do not know the abundances of other expected constituents of the lunar exosphere but upper limits exist for many [*Stern*, 1999]. *Wurz et al.* [2007] and *Sarantos et al.* [2012] estimated abundances for these undetected species by assuming thermal desorption, impact vaporization, and sputtering sources, respectively. Both of these studies concluded that models for many refractory gases are not well-constrained by existing measurements. In their study, *Sarantos et al.* [2012] found that: a) the published upper limits for Mg and Fe greatly exceed the expected production by micrometeoroids and the solar wind; b) the modeled Al and O column abundances from these sources are comparable to present upper limits; c) the modeled column abundance for Si and Ti is higher than published limits by a factor of four to six, and d) the calculated Ca abundance

123 was much higher than the upper limit. The low upper limit for Si and Ti was due to
124 measurements of lines corresponding to excited states that are unlikely to be populated.
125 Additionally, the low upper limit for Ca could be interpreted as consistent with increased
126 loss to condensation and molecular formation in the impact cloud. Because of significant
127 uncertainties in microphysical parameters for the sources and losses, *Sarantos et al.*
128 [2012] concluded that the predicted abundances of exospheric refractories are probably
129 upper limits.

130 Figure 1 presents the estimated distribution of twelve lunar neutral species.
131 Estimates for He were provided by models of *Hartle and Thomas* [1974], and estimates
132 for Na by *Sarantos et al.* [2010]. Models for these two species have been validated with
133 measurements. Estimates for the gaseous abundances of the main regolith constituents
134 (O, Si, Al, Ca, Mg, K, Ti, and Fe) were obtained by *Sarantos et al.* [2012]. This model
135 assumed that the surface reservoir is uniform, that K is released by PSD with cross-
136 sections and temperatures similar to that of Na, that refractories are released by the
137 combination of ion sputtering and impact vaporization, and that all particles stick upon
138 contact with the surface. Models for those species compared favorably to upper limits
139 except for Ca; for that species we produced ions consistent with the upper limits [*Stern,*
140 1999]. Because we do not have appropriate models for the production and loss of some
141 expected volatiles, such as C and S, we used a spatially uniform *Chamberlain* [1963]
142 model assuming the ejecta temperature of 400 K and the exospheric abundance at low
143 altitudes given by *Stern* [1999]. We do not present a model for Ar.

144 Pickup ions formed from the ionized neutral exosphere were tracked in the
145 interplanetary electric and magnetic fields. Photoionization rates for these species were
146 estimated from cross-sections by *Verner et al.* [1996]. The motion of lunar ions under
147 **E**×**B** drift can be obtained analytically (i.e., using constants of motion) when they travel
148 in spatially uniform magnetic and electric fields. Under these conditions, *Hartle et al.*
149 [2011] employed the Vlasov equation with an ion source term to derive an expression for
150 the phase space density, *f*, of pickup ions that accounts for the three-dimensional
151 distribution of the neutral source gas. With this approach, a given ion velocity vector, **v**,
152 arrives at a location **r** with a probability density $f(\mathbf{r},\mathbf{v})$ that relates to the neutral density
153 back to its point of origin, $\mathbf{r_0}$, through the expression:

154 $$f(\vec{\mathbf{r}},\vec{\mathbf{v}}) = \frac{2r_g R}{V_d^3}\delta(v_x^2 + v_y^2 - 2v_x) \sum_{\substack{all\ Cycloids \\ (\mathbf{r},\mathbf{v})\rightarrow(\mathbf{r_0},\mathbf{v_0}=0)}} N(\vec{\mathbf{r}}_0) \quad (1)$$

155 Here r_g is the ion gyroradius; R the photoionization rate; $V_d = |\mathbf{E} \times \mathbf{B}| / B^2$ the
156 bulk drift velocity of an ion in magnetic and electric fields **B** and **E**, respectively; $N(\mathbf{r_0})$
157 the neutral density at each point of origin; v_y the instantaneous ion velocity along **E** at
158 location **r**, and v_x is the instantaneous ion velocity along the drift direction. The delta
159 function indicates that *f* is a function of just one component of the ion velocity because
160 under these assumptions ions move perpendicular to the magnetic field ($v_z = 0$) and
161 remain in a ring velocity distribution. Some velocities in Eq. (1) are less probable to be
162 observed because they originated farther upstream, where the neutral density and the
163 production rate of new ions are small. The summation includes all cycloids that
164 originated several gyroradii upstream and arrive at the point of interest with the same
165 velocity, *v*. In practice, only one to two cycloids must be included in the summation

166 because the gyroradii of lunar ions greatly exceed the neutral scale heights. Eq. (1) with
167 N from our neutral models can be used to numerically compute how ions from the lunar
168 exosphere map into an ion spectrometer. Integrals of the distribution function (1) over the
169 allowed velocity space yield densities, velocities, and macroscopic fluxes at any location
170 above the surface for arbitrary Interplanetary Magnetic Field (IMF) and solar wind
171 directions.

172 The formulation adopted here (Eq. 1) assumes that the solar wind flow direction
173 and magnetic field are spatially uniform, assumptions that are good approximations in the
174 lunar dayside, but not in the lunar wake nor near the highly electrically charged lunar
175 terminators. The simplifying assumptions of the ion transport model ignore the effects of
176 wave-particle interactions, which may scatter ions in velocity space and remove them
177 from a ring distribution, as well as the presence around the Moon of magnetic anomalies.
178 Given these limitations, our estimates are valid only for the lunar dayside.

179

180 4. Model Predictions

181 Figure 2a presents estimates for the ion flux of 12 expected exospheric constituents.
182 These estimates were produced at 100 km, the orbital altitude of Kaguya, for a Parker
183 spiral IMF configuration (field in the ecliptic, 45° off the Sun-Moon line), with a
184 component away from the Sun and a magnitude of 8 nT. The assumed solar wind velocity
185 was 400 km/s in these simulations. A realistic range for the expected fluxes of exo-ions
186 can be obtained if estimates of omni-directional flux at two locations above the Moon are
187 provided: at the subsolar point (blue), and at a point above the surface where the flux is
188 maximum (red), a location away from the subsolar point in the direction of the electric

189 field (see Figure 3). Fluxes from the exosphere are compared in Fig. 2b to the secondary
190 ion flux leaving the surface [*Elphic et al.*, 1991] due to solar wind bombardment at a flux
191 typical of the solar wind at 1 AU, 4×10^8 cm^{-2} s^{-1}. Based on these predictions, we
192 conclude that the exo-ion rates for many of these species, especially Al^+ and Si^+, greatly
193 exceed the secondary ion rates. Hence, it should be possible to constrain the unknown
194 levels of some lunar neutrals with ion spectrometer data.

195 Now consider the spatial distribution of ions originating from the exosphere and
196 their arrival into an instrument. Here we focus on the two best-specified neutral species in
197 our model, He and Na. The exo-ion flux at an altitude of 100 km above the lunar dayside
198 is plotted in Figure 3. Shown on the left (panels 3a and 3c) is the omni-directional flux of
199 exospheric He^+ and Na^+ as a function of Selenocentric Solar Ecliptic (SSE) longitude and
200 latitude, with the subsolar point denoted by a white dot. Fluxes of dayside He^+ peak near
201 the terminator because He neutrals are more abundant on the cooler terminator [*Hartle*
202 *and Thomas*, 1974]. The flux of exo-ions peaks in the quadrant that lies in the direction
203 of the electric field because at these locations we probe the lower volume (<100 km) of
204 the exosphere (see Fig. 4 of *Hartle and Killen* [2006] for a visual explanation).

205 The actual flux calculations are contrasted in Fig. 3b and 3d to the flux of the
206 same two species that would be observed by a 2π detector pointing nadir - like the MAP-
207 PACE-IMA spectrometer onboard Kaguya. Ions from the exosphere map inefficiently
208 into the nadir-pointing mass spectrometer in the quadrant against the direction of the
209 solar wind electric field. This is because freshly picked-up ions lie near the electric field
210 direction, which for this IMF configuration is excluded from the instrument's field of

211 view in the region over southern latitudes. A higher fraction of the total exo-ion flux is
212 recorded elsewhere, with the portion of phase space density seen varying as a function of
213 spacecraft location. The region northward of the white dotted lines in Panels a-d is the
214 region over which both surface and exospheric ions map into the instrument. Counts
215 below this line can be uniquely identified with an exospheric origin. Integrating the
216 expected signal from exospheric and surface ions over the Sun-Moon meridian to
217 approximate the geometry of a polar orbiter like Kaguya, the model estimates that
218 $Na^{+}_{exosphere} > 7 \times Na^{+}_{surface}$ and $Al^{+}_{exosphere} > 30 \times Al^{+}_{surface}$ for the *Elphic et al.* [1991]
219 yields and a solar zenith angle dependence for sputtered ions. Therefore, both local
220 (instantaneous) spectra and spectra integrated over a dayside pass by the Kaguya IMA
221 can be used to determine the relative composition of the exosphere.

222 Our simulations indicate that some constituents of the exo-ionosphere
223 map into Kaguya IMA better than others, biasing the spectrum measured for a given orbit
224 and IMF configuration. For example, Figure 4a shows the actual (omni-directional)
225 Na^{+}/He^{+} flux ratio as a function of selenocentric location at an altitude of 100 km. The
226 expected Na^{+} flux for a Parker IMF is about twice that of He^{+} at subsolar locations, while
227 the He^{+} flux exceeds that for Na^{+} by about a factor of ten on some locations near the
228 terminator. Figure 4b shows the relative Na^{+}/He^{+} flux ratio for a virtual 2π nadir
229 instrument like Kaguya IMA. Over large portions of the hemisphere on the side of the
230 electric field, IMA would report a correct ratio, but, near the subsolar point, the relative
231 abundance of Na^{+}/He^{+} measured by IMA would be higher than actual. Panels c and d of
232 Figure 4 clarify that whereas the velocity distribution of Na^{+} is sharply peaked, that of
233 He^{+} is wider, and more of it is excluded from the instrument over the subsolar point. In

234 contrast, over other locations, where Kaguya IMA cannot observe near the direction of
235 the E-field, it would record a relatively higher portion of He^+. Because of these effects, if
236 spectra integrated over a whole meridian are studied (Fig. 4e), the amount of He^+ relative
237 to Na^+ would be overestimated on the dayside for this IMF configuration. Therefore,
238 Kaguya IMA spectra must be carefully interpreted orbit by orbit before accurate
239 estimates of relative abundance can be made.

240 5. Conclusions

241

242 Both surface and exospheric ions contribute to the lunar environment. Ti^+, Fe^+,
243 Mg^+, and especially Ca^+ are mainly ejected from the surface. For the other species studied
244 here, ionization of the exospheric constituents could result in fluxes that significantly
245 exceed the surface production rate. In our model, which predicts levels for neutral Al and
246 Si near the upper limits observed by telescopes, Al^+ and Si^+ would be the dominant
247 pickup ions species around the Moon, similar to what was observed by the AMPTE
248 spacecraft [*Hilchenbach et al, 1991*]. Hence, we predict that Al and Si should be the most
249 easily constrainable neutral species by ion measurements.

250 We cannot explain the reported overabundance of observed O^+ relative to other
251 species (roughly 3:1 count ratio between peaks corresponding to masses 16 and 28 in
252 *Mall et al.*, 1998) with neutral oxygen release at levels expected from impacts and solar
253 wind sputtering. This conclusion is reached even though our neutral model prediction for
254 O is essentially at the upper limits from measurements by Apollo 17 of the oxygen triplet
255 [Table 2 of *Sarantos et al.*, 2012 and references therein]. No O^+ was detected in sputtered
256 ion experiments [*Elphic et al., 1991*] and little was detected in ESD experiments [*McLain*

257 *et al., 2011*], making a surface origin for O^+ unlikely. If a lunar origin of the O^+ observed
258 is posited, volatile molecular ions such as OH^+, H_2O^+, CO^+ or CO_2^+ may be contributing
259 to the O^+ and C^+ measured by Kaguya and WIND, a possibility suggested by *Tanaka et*
260 *al.* [2009] that would help mitigate the model-data discrepancy for O^+.

261 Our estimate of lunar O^+ fluxes, $\sim 4 - 6 \times 10^3$ ions cm^{-2} s^{-1}, suggests the
262 possibility of significant contributions by Earth outflow to measurements obtained with
263 the Moon inside the terrestrial magnetosphere. A model of the O^+ outflow from Earth
264 [*Glocer et al.*, 2009], run for conditions prevailing on April 20, 2008, the day of the
265 observations reported by *Tanaka et al* [2009], predicts that $\sim 3 \times 10^3$ ions cm^{-2} s^{-1} reach
266 the Earth's magnetic lobes at the distance of 60 Earth radii. Earth's polar wind ions may
267 affect the lunar environment even more significantly during geomagnetically active
268 conditions.

269 Discrepancies found between the simulated and observed ion spectra can further
270 our understanding of the lunar environment, especially as new measurements of lunar
271 ions by the Acceleration, Reconnection, Turbulence, and Electrodynamics of the Moon's
272 Interaction with the Sun (ARTEMIS) [*Sibeck et al.*, 2011], and of lunar neutrals by the
273 Lunar Reconnaissance Orbiter (LRO) and the Lunar Atmosphere and Dust Environment
274 Explorer (LADEE), become available over the next couple of years.

275

276 Acknowledgments: MS, REH, and RMK acknowledge funding from the NASA Lunar
277 Science Institute, DREAM.

278

279

280 References

281

282 Chamberlain, J. W. (1963), Planetary corona and atmospheric evaporation, *Planet. Space*
283 *Sci.*, 11, 901 – 960.

284 Elphic, R. C., H. O. Funsten, B. L. Barraclough, D. J. McComas, M. T. Paffet, D. T.
285 Vaniman, and G. Heiken (1991), Lunar surface composition and solar wind – induced
286 secondary ion mass spectrometry, *Geophys. Res. Lett.*, 18, 2165–2168.

287 Glocer, A., G. Tóth, Y. Ma, T. Gombosi, J.-C. Zhang, and L. M.
288 Kistler (2009), Multifluid Block-Adaptive-Tree Solar wind Roe-type Upwind
289 Scheme: Magnetospheric composition and dynamics during geomagnetic storms—
290 Initial results, *J. Geophys. Res.*, *114*, A12203, doi:10.1029/2009JA014418.

291 Hartle, R. E. and G. E. Thomas (1974), Neutral and ion exosphere models for lunar
292 hydrogen and helium, *J. Geophys. Res.*, 79, 1519 – 1526.

293 Hartle, R. E., and R.M. Killen (2006), Measuring pickup ions to characterize the surfaces
294 and exospheres of planetary bodies: Applications to the Moon, *Geophys. Res. Lett.*,
295 33, L05201, doi: 10.1029/2005GL024520.

296 Hartle, R.E., M. Sarantos, and E. C. Sittler (2011), Pickup ion distributions from three-
297 dimensional neutral exospheres, *J.. Geophys. Res*, 116, A10101, doi:
298 10.1029/2011JA016859.

299 Hilchenbach, M., D. Hovestadt, B. Klecker, and E. Moebius (1991), Detection of singly
300 ionized energetic lunar pick-up ions upstream of earth's bow shock, in *Solar Wind*
301 *Seven*, edited by E. Marsch and G. Schwenn, 150-155, Pergamon, New York.

302 Mall, U., E. Kirsch, K. Cierpka, B. Wilken, A. Söding, F. Neubauer, G. Gloeckler, and A.
303 Galvin (1998), Direct observation of lunar pick-up ions near the Moon, *Geophys. Res.*
304 *Lett.* 25, 3799-3802.
305 McLain, J. L., A.L. Sprague, G.A. Grieves, D. Schriver, P. Travnicek, and T.M. Orlando
306 (2011), Electron-stimulated desorption of silicates: A potential source for ions in
307 Mercury's space environment, *J.. Geophys. Res.*, 116, E03007.
308 Saito, Y., et al. (2010), In-flight Performance and Initial Results of Plasma Energy Angle
309 and Composition Experiment (PACE) on SELENE (Kaguya), *Spa. Sci. Rev.*, 154,
310 265 – 303.
311 Sarantos, M., R.M. Killen, A.S. Sharma, and J.A. Slavin (2010), Sources of sodium in the
312 lunar exosphere: Modeling using ground-based observations and spacecraft data of
313 the plasma, *Icarus,* 205, 364-374.
314 Sarantos, M., R. M. Killen, D. Glenar, M. Benna, and T. J. Stubbs (2012), Metallic
315 species, oxygen and silicon in the lunar exosphere: upper limits and prospects for
316 LADEE measurements, *J. Geophys. Res.*, 117, A03103, doi:10.1029/2011JA017044.
317 Sibeck, D.G., et al. (2011), ARTEMIS Science Objectives, *Space Sci. Rev.*, 165, 59-91.
318 Stern, S.A. (1999), The lunar atmosphere: history, status, current problems, and context,
319 *Rev. Geophys.*, 37, 453 – 491.
320 Tanaka, T., et al. (2009), First in situ observation of the Moon-originating ions in the
321 Earth's Magnetosphere by MAP-PACE on SELENE (KAGUYA), *Geophys. Res. Lett.*
322 36, L22106, 10.1029/2009GL040682.

323 Verner, D. A., G.J. Ferland, K.T. Korista, and D.G. Yakovlev (1996), Atomic Data for
324 Astrophysics. II. New Analytic FITS for Photoionization Cross Sections of Atoms
325 and Ions, *Astrophys. J.* 465, 487 – 498.
326 Wurz, P., U. Rohner, J.A. Whitby, C. Kolb, H. Lammer, P. Dobnikar, and J.A. Martín-
327 Fernández (2007), The lunar exosphere: The sputtering contribution, *Icarus, 191*,
328 486-496.
329 Yokota, S., and Y. Saito (2005), Estimation of picked-up lunar ions for future
330 compositional remote SIMS analyses of the lunar surface, *Earth Planets Space*, 57,
331 281-289.
332 Yokota, S., et al. (2009). First direct detection of ions originating from the Moon by
333 MAP-PACE IMA onboard SELENE (KAGUYA), *Geophys. Res. Lett.* 36, L11201,
334 doi:10.1029/2009GL038185.
335

336

337 **Figure Captions**

338 **Figure 1**. Neutral profiles above the subsolar point that are adopted in our simulations.

339 **Figure 2**. Relative importance of exospheric and surface sources of lunar pickup ions. (a)
340 Flux range of ions from the exosphere computed at a dayside altitude of 100 km over two
341 selenocentric locations, the subsolar point (blue), and a location of maximum flux (red);
342 (b) flux of ions from the surface due to solar wind impact (from *Elphic et al., 1991*).
343 Fluxes were computed for a Parker spiral IMF configuration of 8 nT, the solar wind
344 speed of 400 km/s, and the density of 10 protons cm^{-3}.

345 **Figure 3**. Distribution of He^+ and Na^+ of exospheric origin on the lunar dayside (alt=100
346 km): (left) omni-directional flux; (right) flux that maps into a nadir pointing 2π detector,
347 a proxy for the Kaguya IMA. Both surface and exospheric ions map onto a spacecraft
348 north of the white dotted lines, but surface ions are excluded from this calculation.

349 **Figure 4**. Exospheric Na^+/He^+ ratio that would be locally measured at a dayside altitude
350 of 100 km by (a) a 4π detector; (b) a nadir pointing 2π detector. The velocity distribution
351 function (VDF) of ions arriving at the detector, in normalized units, is shown as a
352 function of the electric field direction over two locations at this altitude, (c) a location
353 near equatorial dawn, and (d)a location near the subsolar point. The portion of velocity
354 space not seen by the nadir pointing 2π detector is shaded. Because the fraction of flux
355 measured varies with species and location, (e) exo-ion spectra integrated along any
356 meridian would lead to underestimation by Kaguya IMA (red line) of Na^+ relative to He^+
357 for this IMF orientation.

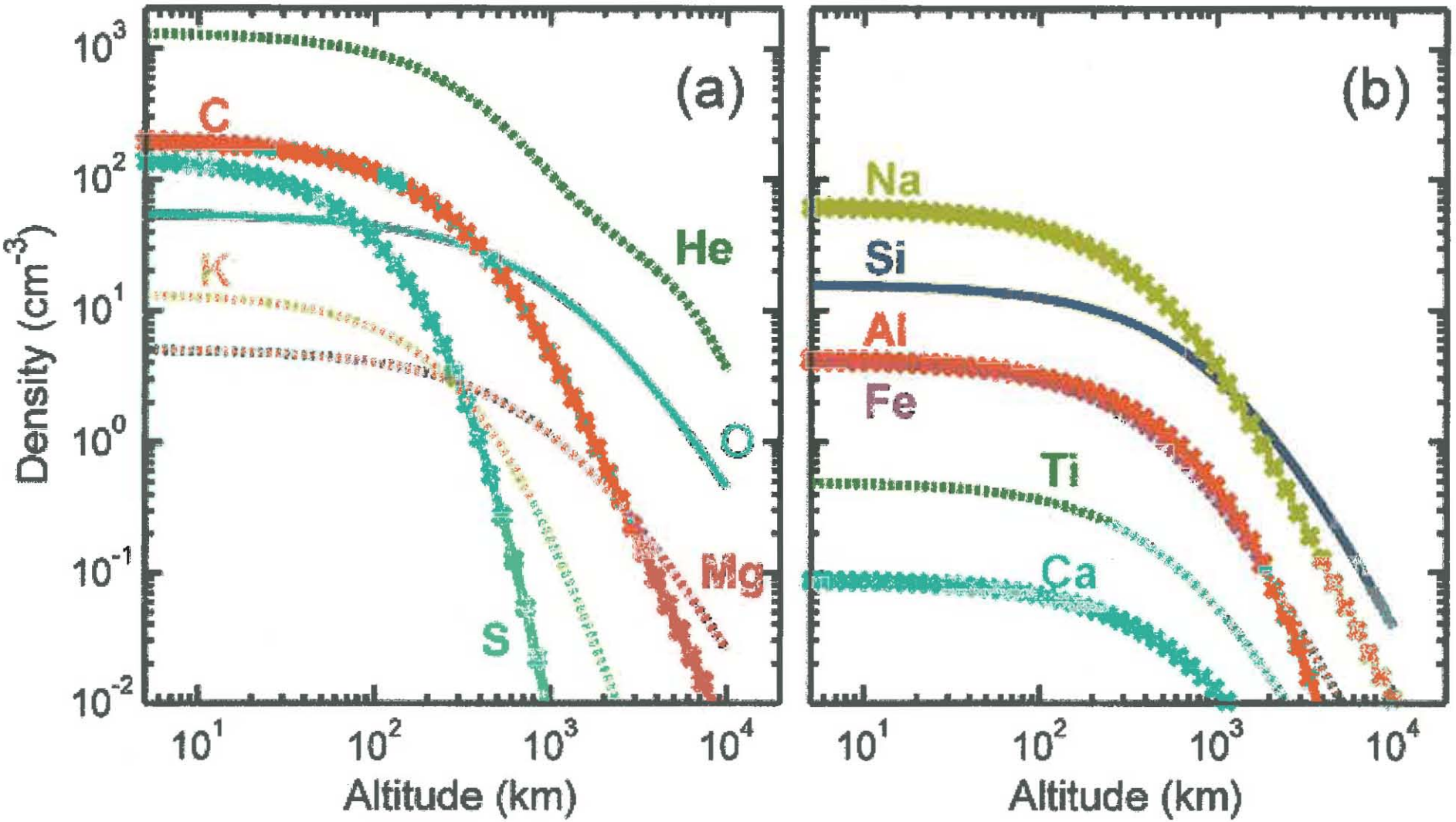
(a)
(b)
Density (cm^{-3})
Altitude (km)
Altitude (km)
C
He
K
O
Mg
S
Na
Si
Al
Fe
Ti
Ca
10^3
10^2
10^1
10^0
10^{-1}
10^{-2}
10^1
10^2
10^3
10^4

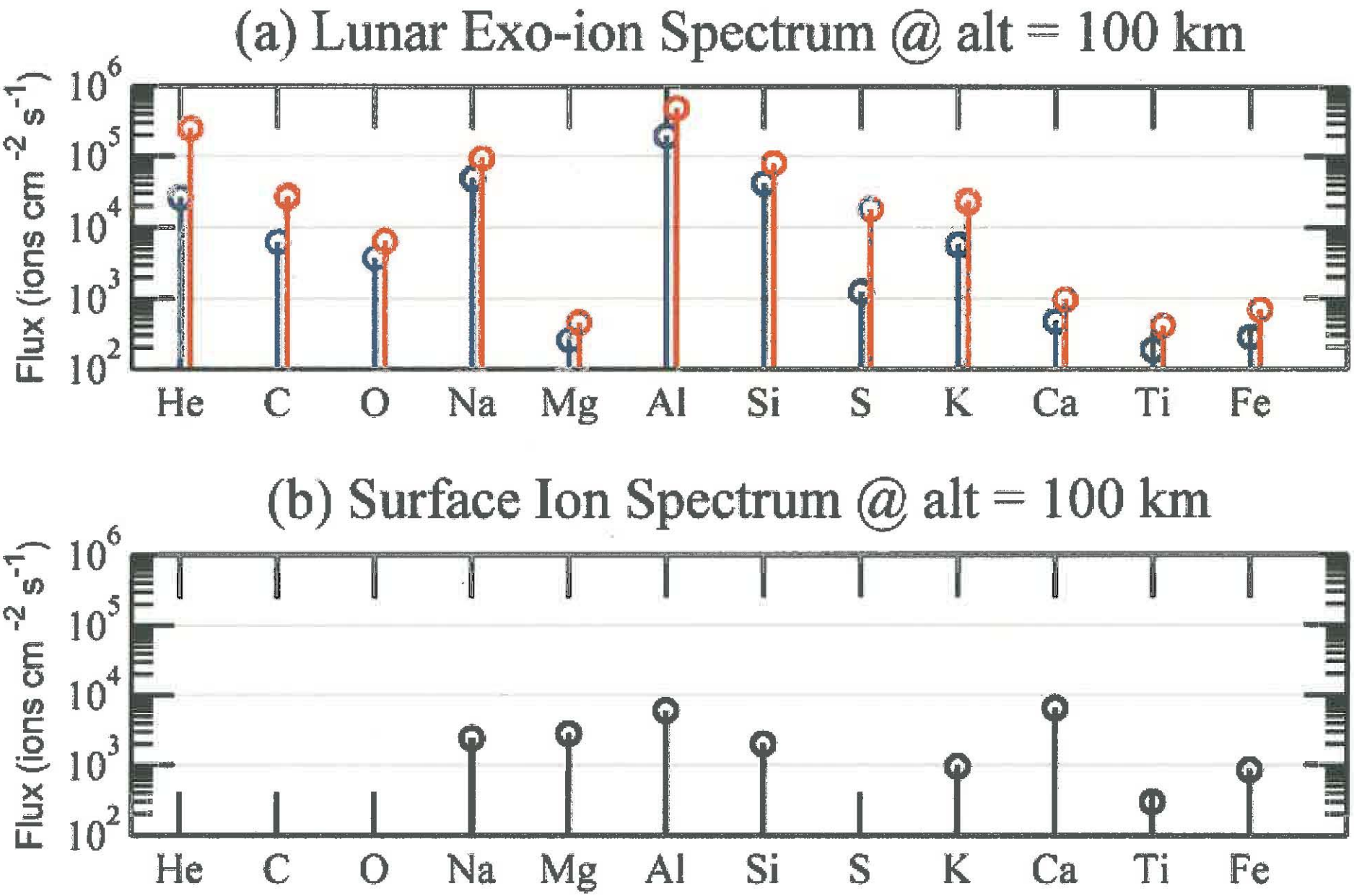
(a) Lunar Exo-ion Spectrum @ alt = 100 km
Flux (ions cm -2 s-1)
10^6
10^5
10^4
10^3
10^2
He C O Na Mg Al Si S K Ca Ti Fe
(b) Surface Ion Spectrum @ alt = 100 km
Flux (ions cm -2 s-1)
10^6
10^5
10^4
10^3
10^2
He C O Na Mg Al Si S K Ca Ti Fe

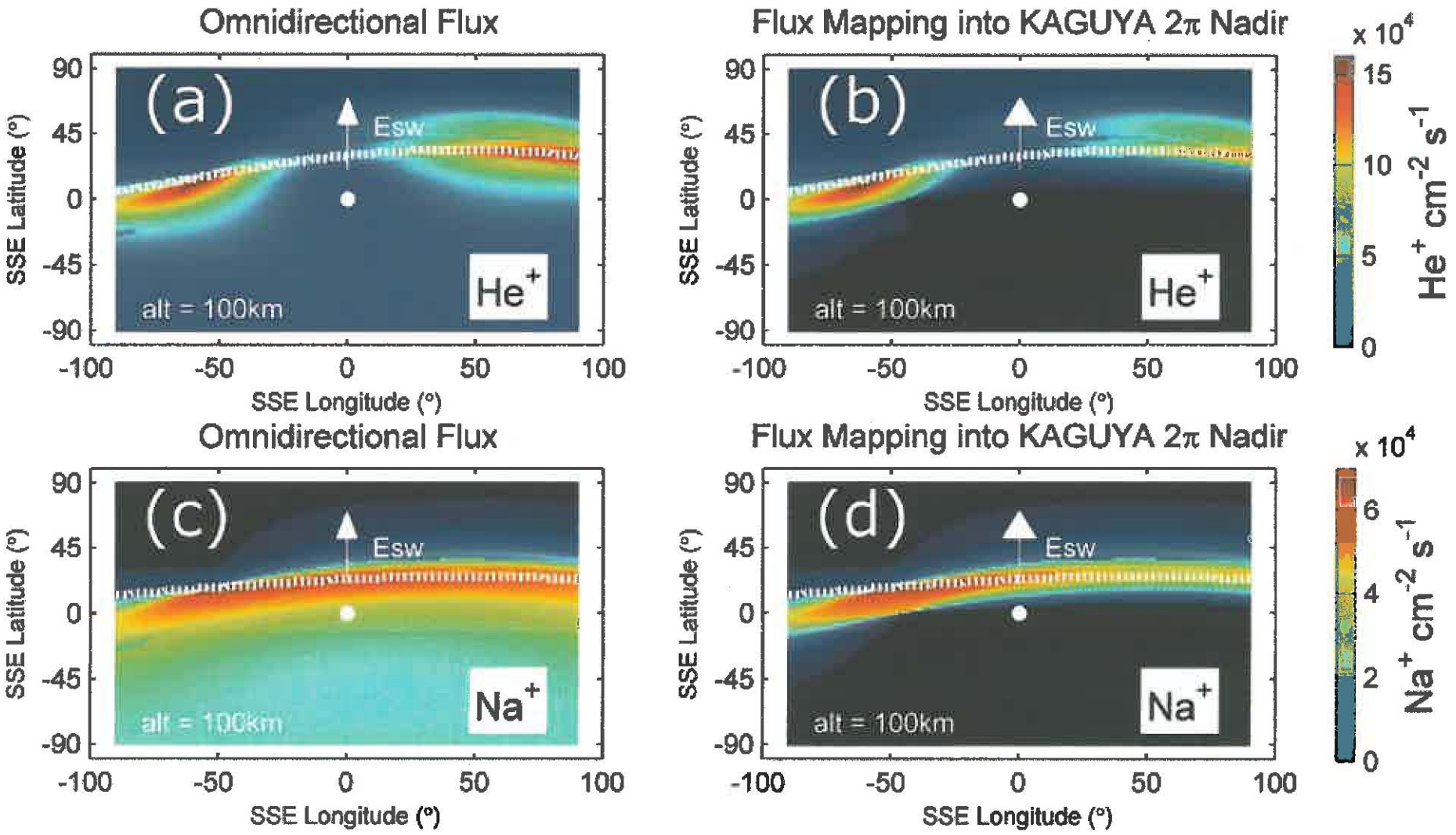
Omnidirectional Flux
Flux Mapping into KAGUYA 2π Nadir
(a)
(b)
(c)
(d)
Esw
alt = 100km
He+
Na+
SSE Latitude (°)
SSE Longitude (°)
90
45
0
-45
-90
-100
-50
0
50
100
x 10^4
15
10
5
0
6
4
2
He+ cm-2 s-1
Na+ cm-2 s-1

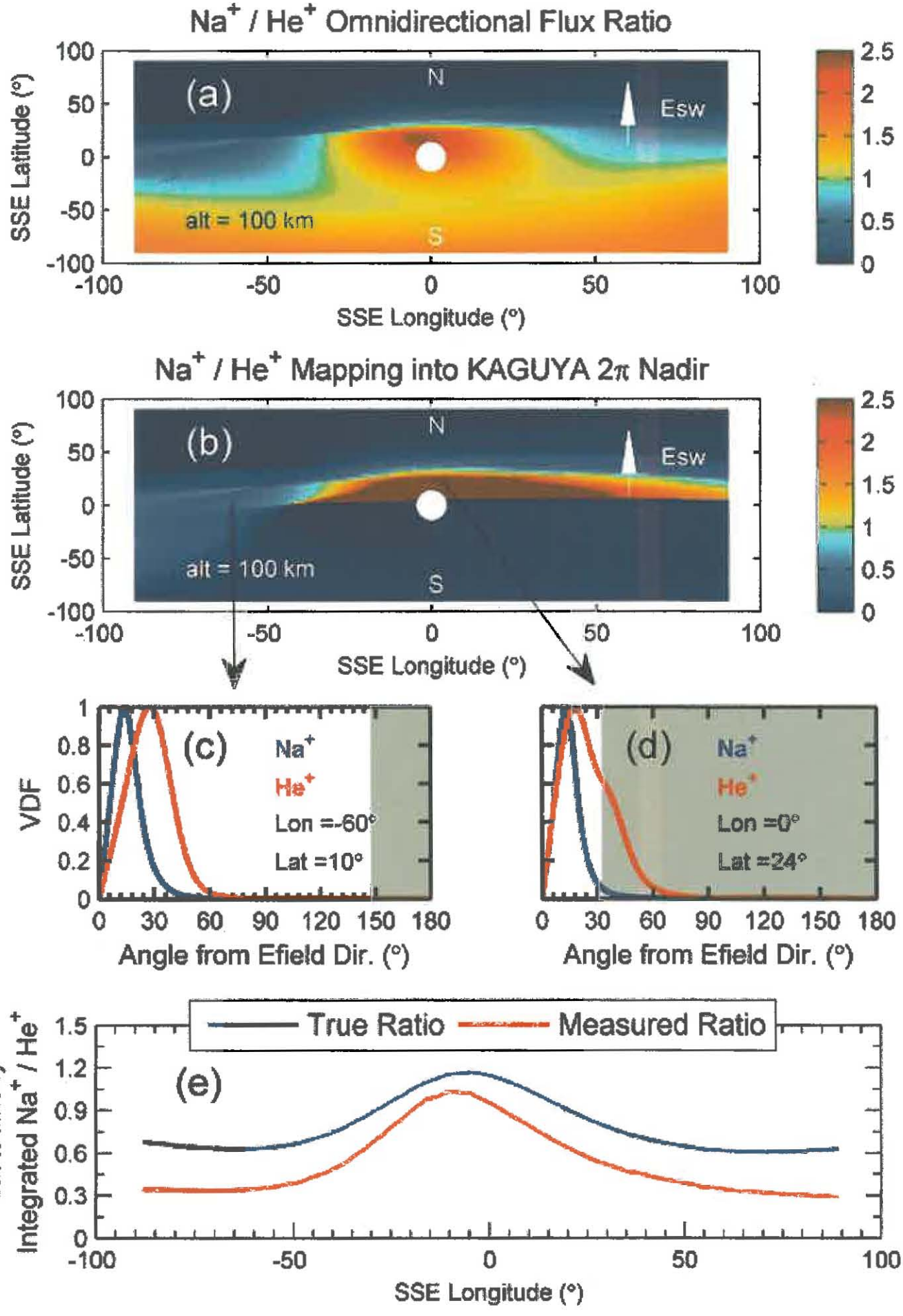
Na+ / He+ Omnidirectional Flux Ratio
(a)
N
Esw
alt = 100 km
S
SSE Latitude (°)
SSE Longitude (°)
Na+ / He+ Mapping into KAGUYA 2π Nadir
(b)
(c)
(d)
Na+
He+
Lon =-60°
Lat =10°
Lon =0°
Lat =24°
VDF
Angle from Efield Dir. (°)
True Ratio
Measured Ratio
(e)
Latitudinally Integrated Na+ / He+